

# The catabolic specialization of the marine bacterium *Polaribacter* sp. Q13 to red algal $\beta$ 1,3/1,4-mixed-linkage xylan

Fang Zhao,<sup>1</sup> Chun-Mei Yu,<sup>1</sup> Hai-Ning Sun,<sup>1</sup> Ting-Ting Xu,<sup>1</sup> Zhong-Zhi Sun,<sup>1</sup> Qi-Long Qin,<sup>1</sup> Ning Wang,<sup>1</sup> Xiu-Lan Chen,<sup>1,2,3</sup> Yang Yu,<sup>1</sup> Yu-Zhong Zhang<sup>1,2,3</sup>

**AUTHOR AFFILIATIONS** See affiliation list on p. 14.

**ABSTRACT** Catabolism of algal polysaccharides by marine bacteria is a significant process of marine carbon cycling.  $\beta$ 1,3/1,4-Mixed-linkage xylan (MLX) is a class of xylan in the ocean, widely present in the cell walls of red algae. However, the catabolic mechanism of MLX by marine bacteria remains elusive. Recently, we found that a marine Bacteroidetes strain, *Polaribacter* sp. Q13, is a specialist in degrading MLX, which secretes a novel MLX-specific xylanase. Here, the catabolic specialization of strain Q13 to MLX was studied by multiomics and biochemical analyses. Strain Q13 catabolizes MLX with a canonical starch utilization system (Sus), which is encoded by a single xylan utilization locus, XUL-Q13. In this system, the cell surface glycan-binding protein SGBP-B captures MLX specifically, contributing to the catabolic specificity. The xylanolytic enzyme system of strain Q13 is unique, and the enzymatic cascade dedicates the stepwise hydrolysis of the  $\beta$ 1,3- and  $\beta$ 1,4-linkages in MLX in the extracellular, periplasmic, and cytoplasmic spaces. Bioinformatics analysis and growth observation suggest that other marine Bacteroidetes strains harboring homologous MLX utilization loci also preferentially utilize MLX. These results reveal the catabolic specialization of MLX degradation by marine Bacteroidetes, leading to a better understanding of the degradation and recycling of MLX driven by marine bacteria.

**IMPORTANCE** Red algae contribute substantially to the primary production in marine ecosystems. The catabolism of red algal polysaccharides by marine bacteria is important for marine carbon cycling. Mixed-linkage  $\beta$ 1,3/1,4-xylan (MLX, distinct from hetero- $\beta$ 1,4-xylans from terrestrial plants) is an abundant red algal polysaccharide, whose mechanism of catabolism by marine bacteria, however, remains largely unknown. This study reveals the catabolism of MLX by marine Bacteroidetes, promoting our understanding of the degradation and utilization of algal polysaccharides by marine bacteria. This study also sets a foundation for the biomass conversion of MLX.

**KEYWORDS** marine bacteria, Bacteroidetes, mixed-linkage xylan, red algae, xylan utilization loci, marine carbon cycling

Algal polysaccharides are abundant organic matter in the ocean (1, 2). The catabolism of algal polysaccharides by marine bacteria is a key component of marine carbon cycling (3). Moreover, algal polysaccharides are the most promising candidates for biomass conversion (4, 5). Therefore, insights into the catabolism of algal polysaccharides by marine bacteria have attracted increasing attention (6–11). Bacteroidetes have been known as prominent degraders of algal polysaccharides. They are abundant and widely distributed in the ocean (12). Bacteroidetes generally package genes involved in polysaccharide catabolism in polysaccharide utilization loci (PUL) within their genomes (13).

**Editor** Jennifer F. Biddle, University of Delaware, Lewes, Delaware, USA

Address correspondence to Ning Wang, wangxn2092@163.com, Xiu-Lan Chen, cxl0423@sdu.edu.cn, or Yang Yu, yuxinhe1022@163.com.

The authors declare no conflict of interest.

See the funding table on p. 14.

**Received** 26 September 2023

**Accepted** 27 November 2023

**Published** 3 January 2024

Copyright © 2024 American Society for Microbiology. All Rights Reserved.

Xylans are polysaccharides composed of xylose linked by  $\beta$ 1,4- and/or  $\beta$ 1,3-glycosidic bonds (14). Xylans in the ocean are mainly from terrestrial plant detritus and algae (11, 15). Xylans in the cell walls of terrestrial plants are hetero- $\beta$ 1,4-xylans, which are composed of  $\beta$ 1,4-linked xylose with multiple side chains such as  $\alpha$ -L-arabinofuranose, 4-O-methyl-glucuronic acid, or acetate (16, 17). Marine algal xylans with known structures, present in the cell walls of green and red algae, are linear homoxylans, including  $\beta$ 1,3-xylan,  $\beta$ 1,4-xylan, and  $\beta$ 1,3/1,4-mixed-linkage xylan (MLX) (18, 19). Among, MLX contains both  $\beta$ 1,3- and  $\beta$ 1,4-linkages at a ratio of approximately 1:4, and single  $\beta$ 1,3-linkages are irregularly distributed along the  $\beta$ 1,4-linked backbone (Fig. 1A) (19–22). MLX is abundant in red algae, especially in orders Palmariales and Nematiales (19–22), constituting a significant carbon source for marine bacteria.

The catabolism of hetero- $\beta$ 1,4-xylans has been investigated in detail in both animal gut symbionts and marine Bacteroidetes (11, 23–25). Bacteroidetes catabolize hetero- $\beta$ 1,4-xylans through xylan-targeting PULs (XUL). Due to the heterogeneity and complexity of hetero- $\beta$ 1,4-xylans, a large diversity of xylanolytic enzymes, including  $\beta$ 1,4-xylanases,  $\beta$ 1,4-xylosidases, and xylan-debranching enzymes (e.g., feruloyl esterases and  $\alpha$ -L-glucuronidases), is required for their complete degradation (11, 23–25). Analogous to the archetypal starch utilization system (*Sus*), *susC* and *susD* genes, encoding the TonB-dependent receptor and the cell surface glycan-binding protein (SGBP), respectively, are hallmarks of Bacteroidetes XULs (23–26).

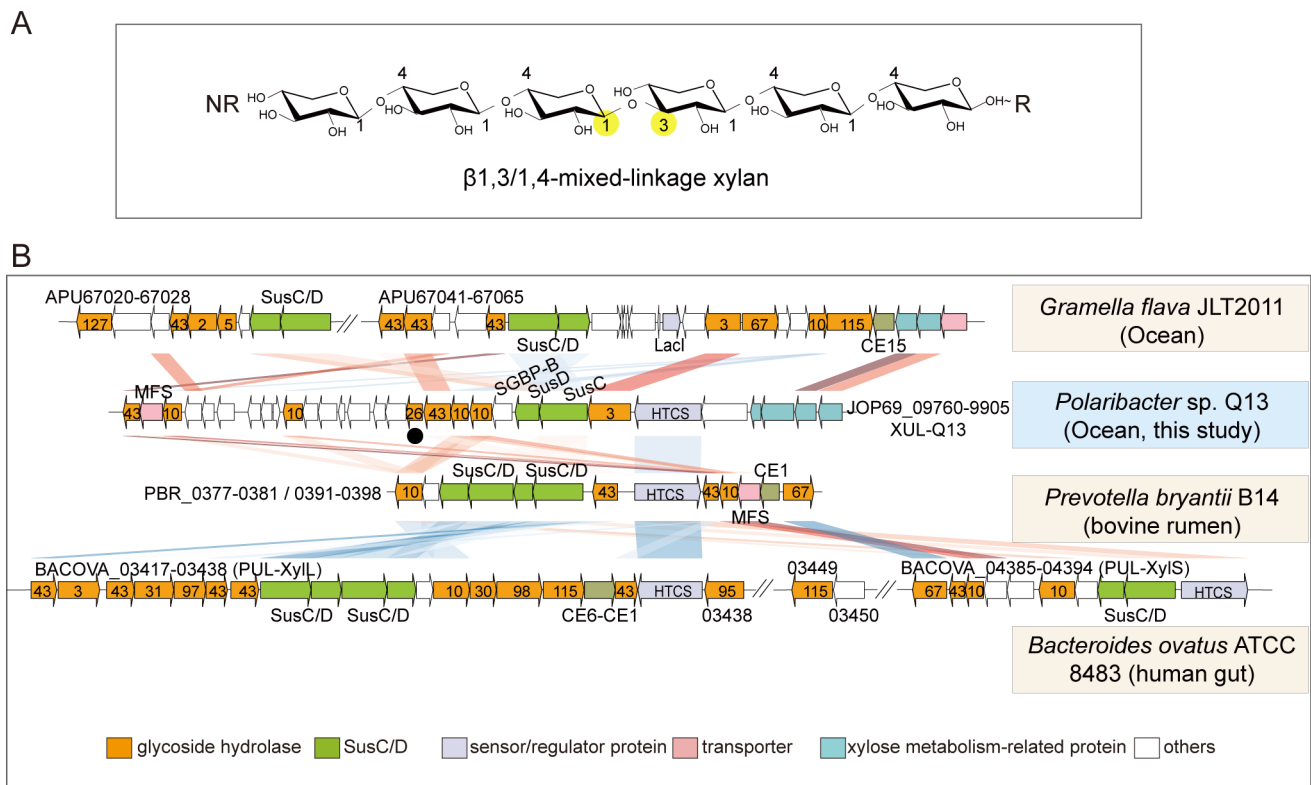
The catabolism of algal xylans, especially MLX, is comparatively less studied. Recently, we found that a marine Bacteroidetes, *Polaribacter* sp. Q13, which was isolated from the surface of red algae collected from Nelson Island, Antarctic, specifically utilizes red algal MLX among different classes of xylans. From this strain, we identified a novel MLX-specific xylanase, Xyn26A, that specifically degrades MLX and produces mixed-linkage xylooligosaccharides (XOs) by attacking the  $\beta$ 1,4-linkages following a  $\beta$ 1,3-linkage toward the reducing end (27). This specificity shares an interesting similarity to that of bacterial  $\beta$ 1,3/1,4-glucanases, which are involved in the catabolism of mixed-linkage  $\beta$ 1,3/1,4-glucan (28). Prior to this study, although a few  $\beta$ 1,3-xylanases and  $\beta$ 1,4-xylanases have been reported to be able to hydrolyze MLX, they are used to elucidate the structure of MLX (29–31). It is unclear whether they are involved in the catabolism of MLX by microorganisms. Therefore, MLX catabolism by marine bacteria is largely unexplored. It is necessary to decipher the complete pathway of MLX catabolism and the mechanism by which strain Q13 preferentially utilizes MLX.

In this study, we provide multiomics and biochemical insights into the catabolism of MLX by strain Q13. This strain catabolizes MLX via an XUL, XUL-Q13. The cell surface glycan-binding protein SGBP-B captures MLX specifically. Then, a distinct xylanolytic enzyme system mediates step-by-step hydrolysis of the  $\beta$ 1,3- and  $\beta$ 1,4-linkages in MLX in the extracellular, periplasmic, and cytoplasmic spaces of strain Q13. The generated xylose is finally assimilated through the xylose isomerase pathway and the pentose phosphate pathway. Furthermore, other marine Bacteroidetes harboring homologous MLX utilization loci were also found to preferentially utilize MLX.

## RESULTS AND DISCUSSION

### Identification of an MLX utilization locus in *Polaribacter* sp. Q13

Strain Q13 is a marine Bacteroidetes that was isolated from the surface of red algae collected from Nelson Island (27). Among structurally diverse xylans from terrestrial plants and marine algae, strain Q13 shows a utilization preference for red algal MLX (27). Genomic analysis of strain Q13 revealed the presence of a putative XUL, XUL-Q13 (locus tag: JOP69\_RS09760-RS09905) (Fig. 1B). To determine the function of XUL-Q13 in MLX catabolism, comparative transcriptome and proteome analyses were performed with MLX and control substrates [xylose (Xyl) and glucose (Glc)], respectively, as the sole carbon source. The results showed that most genes in XUL-Q13 were induced by xylose (compared with glucose) and much more strongly by MLX (Fig. 2A). Similarly, among the three substrates, MLX elicited the strongest expression of most XUL-Q13-encoded

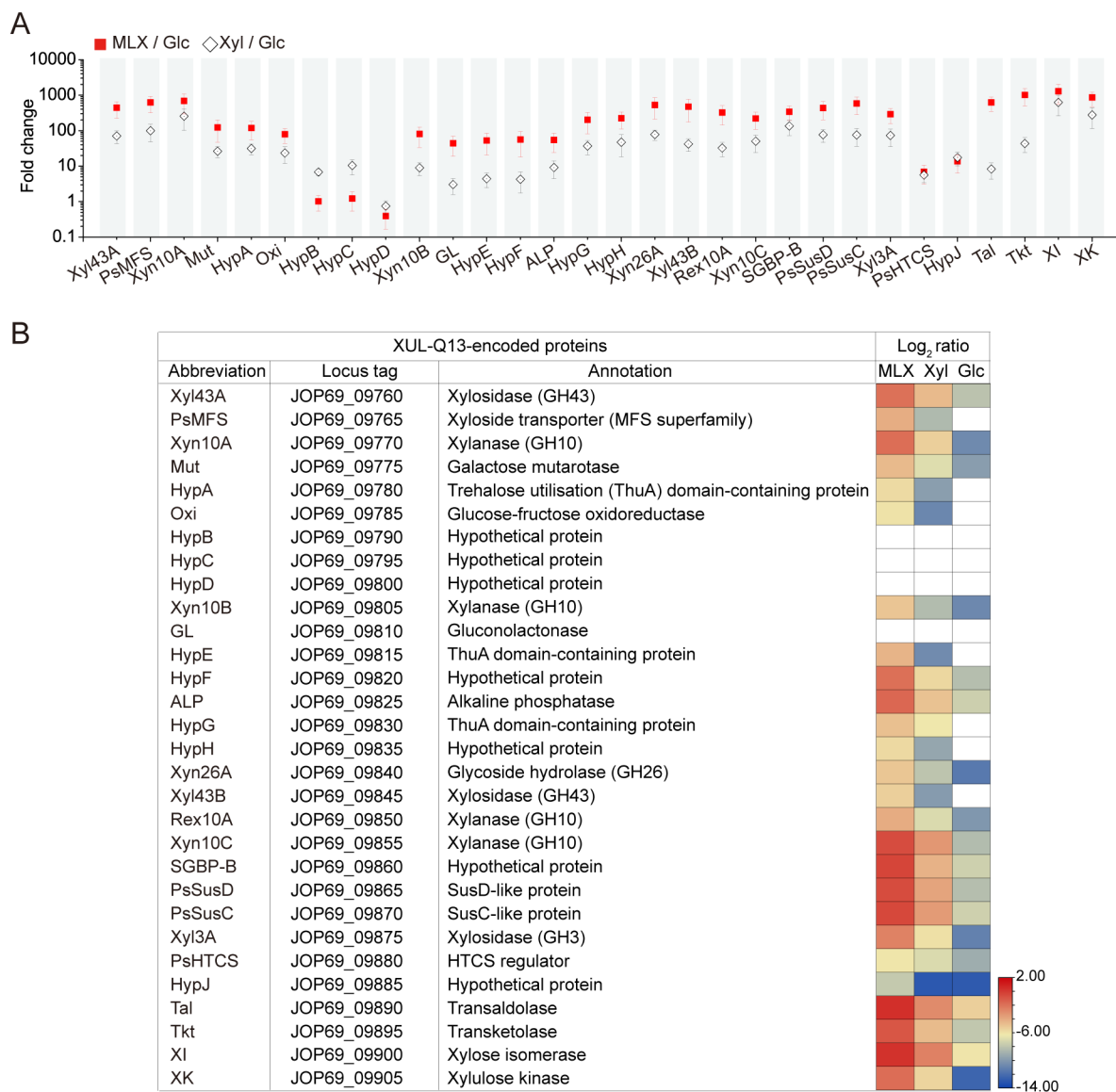


**FIG 1** The xylan utilization locus, XUL-Q13, in *Polaribacter* sp. Q13. (A) Schematic of MLX. The  $\beta$ 1,3-linkage is highlighted with yellow solid circles. NR, non-reducing end; R, reducing end. (B) Synteny of XUL-Q13 and known XULs from animal gut and marine Bacteroidetes. The sequence alignment was performed with BLAST+ (version 2.7.1+,  $E$ -value  $1e-5$ ). Sequence similarities are symbolized by red for direct comparisons and blue for reversed comparisons. Darker colors correspond to higher identities. Numbers labeled in orange arrows indicate GH families. Xyn26A is marked with a solid black circle. HTCS, hybrid two-component sensor; MFS, major facilitator superfamily transporter; CE, carbohydrate esterase.

proteins (Fig. 2B). These results suggest that XUL-Q13 may be involved in MLX catabolism.

XUL-Q13 encodes eight potential xylanolytic enzymes including Xyl43A, Xyn10A, Xyn10B, Xyn26A, Xyl43B, Rex10A, Xyn10C, and Xyl3A (Fig. 2). They belong to glycoside hydrolase (GH) families (<http://www.cazy.org/>) (32) GH3 (Xyl3A), GH10 (Xyn10A, Xyn10B, Xyn10C, and Rex10A), GH26 (Xyn26A), and GH43 (Xyl43A and Xyl43B). The expression of the eight enzymes was all induced by MLX (Fig. 2), suggesting that they likely mediate MLX degradation. GH10 and GH3/43 enzymes are annotated as  $\beta$ 1,4-xylanases and  $\beta$ 1,4-xylosidases, respectively, while Xyn26A has been identified as a novel xylanase that specifically degrades MLX (27). In addition to the enzymes, XUL-Q13 encodes a SusC/D-like transporter complex (PsSucC/PsSucD), an additional non-homologous SGBP (SGBP-B) (described below), a hybrid two-component sensor/regulator (PsHTCS), and an inner membrane xyloside transporter of the major facilitator superfamily (PsMFS) (Fig. 2), suggesting that strain Q13 utilizes MLX through a canonical Sus-like paradigm (13). Moreover, the expression of genes encoding xylose isomerase, xylose kinase, transaldolase, and transketolase, which are located downstream of XUL-Q13, was induced by MLX (Fig. 2), suggesting that xylose is subsequently assimilated through the xylose isomerase pathway and the pentose phosphate pathway (33, 34).

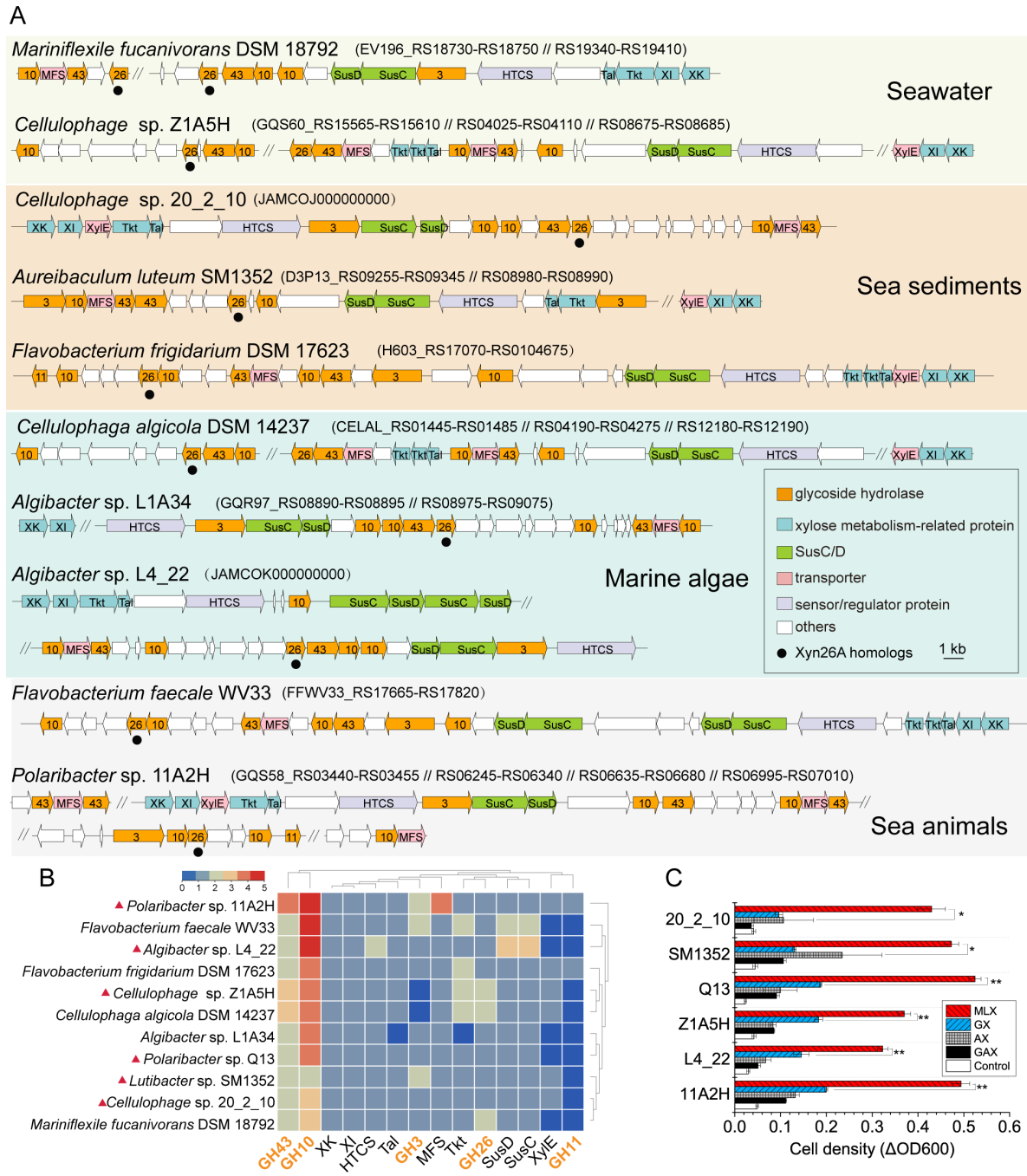
The previously reported XULs from animal gut and marine Bacteroidetes are all associated with the catabolism of hetero- $\beta$ 1,4-xylans (11, 23–25). A comparison of XUL-Q13 with these XULs showed some degrees of synteny, especially genes encoding the SusC/D, HTCS sensor, and MFS transporter (Fig. 1B). However, the MLX-specific xylanase Xyn26A is present in XUL-Q13 but absent from the previously reported XULs (Fig. 1B). Xylan-debranching enzymes present in the previously reported XULs, such as



**FIG 2** Comparative transcriptome (A) and proteome (B) analyses of *Polaribacter* sp. Q13 cells grown on MLX, Xyl, and Glc. Fold changes were calculated from duplicate experiments (mean  $\pm$  SD) with reads per kilobase per million mapped read (RPKM) values of genes expressed in cells grown on MLX and Xyl relative to Glc (MLX/Glc and Xyl/Glc). Log<sub>2</sub> ratios were log-transformed averages of relative intensity-based absolute quantification (riBAQ) values from triplicate experiments. White squares indicate non-quantified proteins.

carbohydrate esterases and  $\alpha$ -L-glucuronidases, are absent from XUL-Q13 (Fig. 1B), corresponding to the homo-structure of MLX. Therefore, despite a canonical Sus-like model, XUL-Q13 encodes a distinct xylanolytic enzyme system.

To identify bacterial XULs similar to XUL-Q13, Xyn26A homologs were searched against all available bacterial genomes in the Integrated Microbial Genomes with Microbiome Samples (IMG/M) database (<https://img.jgi.doe.gov/>) (35), and putative XULs containing at least one Xyn26A homolog and one SusC/D pair were manually screened. Ten bacterial genomes were found, all of which are from marine Bacteroidetes (Fig. 3A). These Bacteroidetes are isolated from marine ecosystems of seawater, sediments, algae, and animals, possessing one or more XULs. These XULs exhibit a similar composition of xylanolytic enzyme systems as XUL-Q13 except that two XULs lack GH3 enzymes and two encode additional GH11 enzymes (annotated as  $\beta$ 1,4-xylanases) (Fig. 3A and B). Similar to strain Q13, all the Bacteroidetes lack xylan-debranching enzymes, implying their inefficiency in utilizing hetero- $\beta$ 1,4-xylans. To investigate whether these



**FIG 3** Occurrence of MLX utilization loci in marine Bacteroidetes. (A) Schematics of MLX utilization loci in marine Bacteroidetes. (B) Co-occurrence analysis of genes in MLX utilization loci of 11 marine Bacteroidetes. The dendrograms shown above and on the right of the heatmap depict the pairwise similarities between rows and columns, respectively. Red solid triangles indicate selected strains for growth studies. (C) Growth of selected marine Bacteroidetes strains on xylans. Cultures without carbon sources were used as controls. \* $P < 0.01$ , \*\* $P < 0.05$  (two-tailed t-test).  $\Delta$ OD<sub>600</sub> values are from triplicate experiments (mean  $\pm$  SD).

Bacteroidetes can utilize MLX, we chose five strains from the genera *Polaribacter*, *Cellulophage*, *Algibacter*, and *Aureibaculum* to test their growth on xylans. The result showed that all the strains preferentially utilized MLX for their growth (Fig. 3C), consistent with the growth profile of strain Q13 on xylans (27), indicating that marine Bacteroidetes containing homologous MLX utilization loci also preferentially utilize MLX.

Together, the catabolism of MLX by strain Q13 is carried out by a single XUL, XUL-Q13. XUL-Q13 is analogous to the known XULs that target hetero- $\beta$ 1,4-xylans but encode

a distinct xylanolytic enzyme system that contains the MLX-specific xylanase Xyn26A. Xyn26A-containing XULs are restricted to marine ecosystems, which is consistent with the fact that MLX is exclusively observed in marine environments (19–22).

### SGBP-B contributes to the catabolic specificity of strain Q13 to MLX

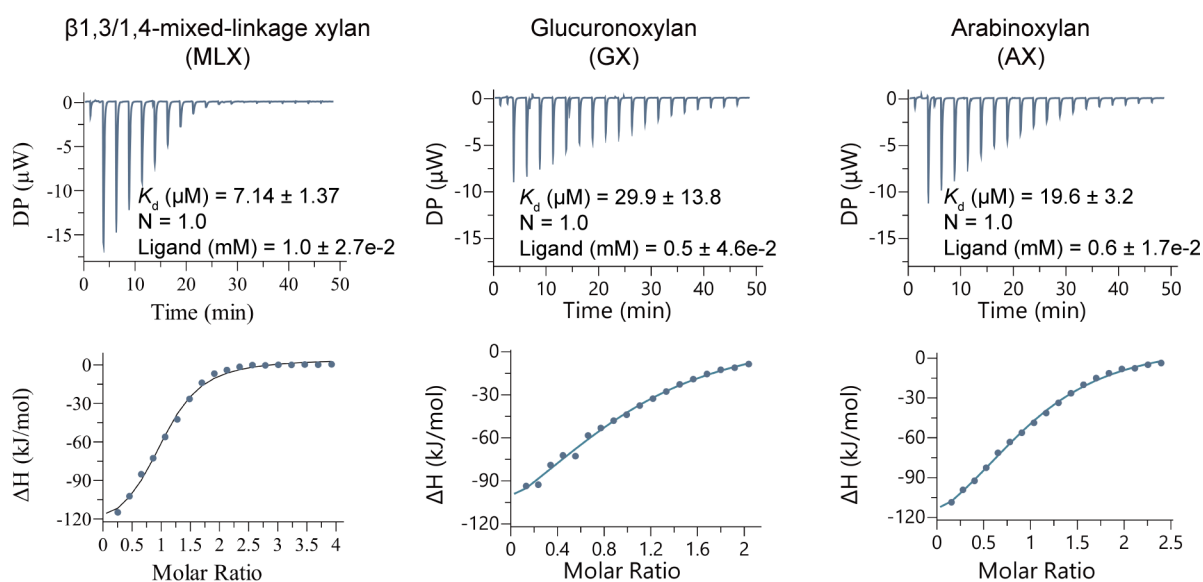
SGBPs are involved in the initial capture of polysaccharides at the cell surface as a prelude to backbone hydrolysis, which contributes to the utilization preference of specific polysaccharides (36, 37). XUL-Q13 encodes two SGBPs, the SusD-like protein PsSusD (also called SGBP-A) and its downstream SGBP-B (Fig. 1B). However, PsSusD bound neither MLX nor hetero- $\beta$ 1,4-xylans [arabinoxylan (GX) or glucuronoxylan (AX)] based on affinity gel electrophoresis and isothermal titration calorimetry (ITC) analyses (data not shown), revealing the inability of PsSusD to recognize xylans. The inability to bind polysaccharides was also previously observed in other SusD-like proteins (37–39).

Based on the conserved domain analysis, SGBP-B is composed of two carbohydrate-binding domains. ITC analysis showed that SGBP-B had a three- to fourfold lower  $K_d$  value for MLX (7.14  $\mu$ M) than hetero- $\beta$ 1,4-xylans GX (29.9  $\mu$ M) or AX (19.6  $\mu$ M), indicating the high affinity of SGBP-B to MLX (Fig. 4). This result suggests that SGBP-B contributes to the catabolic specificity of strain Q13 to MLX.

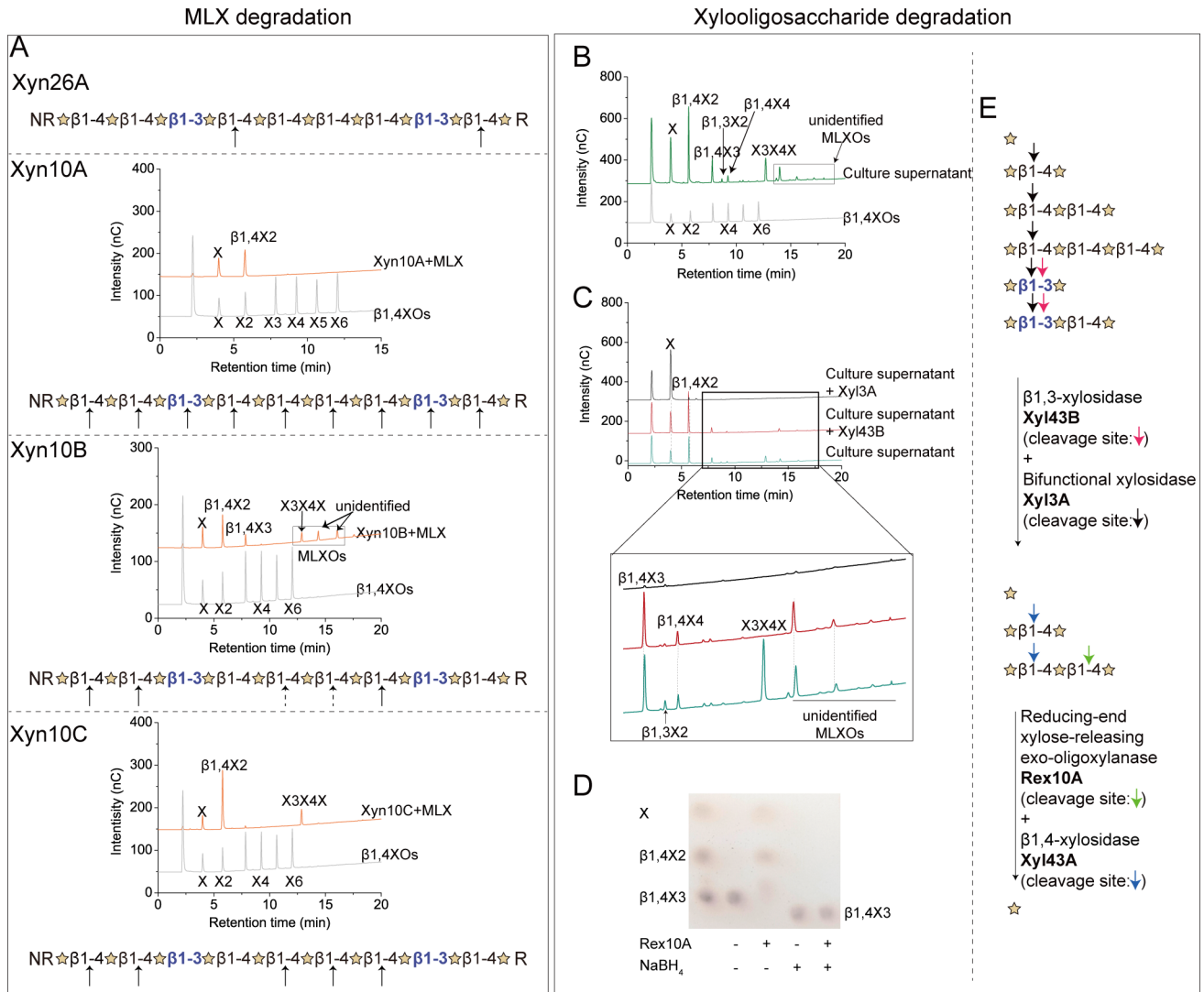
### Degradation of MLX by extracellular xylanases

As mentioned above, XUL-Q13 encodes a distinct xylanolytic enzyme system, which might enable the utilization preference of strain Q13 for MLX. To test this hypothesis, a detailed biochemical investigation was performed with recombinant enzymes that were produced in *Escherichia coli* and purified by Ni-affinity and size exclusion chromatography (SEC) (Fig. S1).

XUL-Q13 encodes four potential extracellular xylanases: Xyn26A, Xyn10A, Xyn10B, and Xyn10C (27) (Fig. 2). Among them, Xyn26A has been shown to be novel xylanase that specifically hydrolyzes the  $\beta$ 1,4-linkages of MLX immediately following a  $\beta$ 1,3-linkage and generates XOs containing one  $\beta$ 1,3-linkage at the reducing end (Fig. 5A) (27). The other three GH10 xylanases all displayed the highest activity at pH 6.0–7.0 and 40°C–50°C (Fig. 6). Substrate specificity analysis showed that the three GH10 xylanases were all active on MLX, GX, and AX (1.1–270.6 U/mg), but inactive on  $\beta$ 1,3-xylan (Fig.




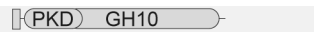


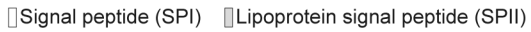
**FIG 4** ITC analysis of the binding capacities of SGBP-B to xylans MLX, GX, and AX. The concentrations of SGBP-B and the ligands were 50  $\mu$ M and 5 mg/mL, respectively. Both SGBP-B and the ligands were prepared in 50 mM Tris-HCl (pH 8.0) containing 100 mM NaCl. Representative data from triplicate experiments are shown. The molar concentration of xylans was estimated to fit  $N$  (binding site) = 1.



**FIG 5** Cascade degradation of MLX by the xylanolytic enzymes of *Polaribacter* sp. Q13. (A) Cleavage sites of xylanases Xyn26A (27), Xyn10A, Xyn10B, and Xyn10C in MLX. The cleavage sites were determined by analyzing the hydrolytic products of xylanases separately. Reaction mixtures containing 90 μL MLX (5 mg/mL) and 10 μL each of xylanases Xyn10A (0.5 mg/mL), Xyn10B (2.4 mg/mL), and Xyn10C (0.6 mg/mL) were incubated at 30°C for 24 h. The products were analyzed by HPAEC-PAD. Xylose, β1,4-xylooligosaccharides (β1,4XOs; β1,4X2-X6), β1,3-xylooligosaccharides (β1,3X2-X3), X3X4X, and X4X3X were used as standards to identify the peaks in chromatograms, and the standard chromatogram of a mixture of xylose and β1,4X2-X6 is shown. The cleavage sites are indicated by arrows, and the indeterminate ones are indicated by dotted arrows. (B) Xylooligosaccharides in the culture supernatant of strain Q13 grown on MLX. Xylose, β1,4-xylooligosaccharides (β1,4XOs; β1,4X2-X6), β1,3-xylooligosaccharides (β1,3X2-X3), X3X4X, and X4X3X were used as standards to identify the peaks in chromatograms, and the standard chromatogram of a mixture of xylose and β1,4X2-X6 is shown. (C) Degradation of xylooligosaccharides in the culture supernatant by periplasmic xylosidases Xyl43B and Xyl3A. A zoom-in view of a part of the chromatogram is shown below. (D) Thin-layer chromatography (TLC) analysis of Rex10A activity on β1,4-xylotriose (β1,4X3) and the reduced β1,4X3 by NaBH<sub>4</sub>. The + and – indicate the presence and absence of the components, respectively. (E) Schematics of the degradation of xylooligosaccharides by periplasmic (Xyl43B and Xyl3A) and cytoplasmic (Rex10A and Xyl43A) enzymes. Cleavage sites are indicated by arrows with different colors. Experiments were performed in triplicate, and representative data are shown. MLXOs, mixed-linkage xylooligosaccharides; unidentified MLXOs, mixed-linkage xylooligosaccharides whose structures were not identified using our available standard xylooligosaccharides.

6), indicating that they are versatile xylanases for both MLX and hetero-β1,4-xylans. Time-course assays showed that within the 24 h hydrolytic process, Xyn10A, Xyn10B, and Xyn10C released initially larger then smaller xylooligosaccharides from MLX (Fig. S2), indicating their endolytic mode of action. To analyze the cleavage site(s) of the three xylanases in MLX, their products released from MLX after 24-h hydrolysis were

Enzyme	Length (amino acid)	$T_{opt}$	$pH_{opt}$	Specific activity (U/mg)				Reference
				Mixed-linkage xylan (MLX)	Glucuronoxylan (GX)	Arabinoxylan (AX)	$\beta$ 1,3-xylan	
Xyn26A		40°C	7.0	204.3 ± 8.5	nd	nd	0.02 ± 0.002	Reference 27
Xyn10A		40°C	6.0-7.0	270.6 ± 9.6	107.2 ± 2.8	87.8 ± 11.1	nd	This study
Xyn10B		40°C	7.0	4.9 ± 0.3	1.1 ± 0.01	1.2 ± 0.1	nd	This study
Xyn10C		50°C	6.0	106.7 ± 2.9	57.0 ± 1.4	85.2 ± 2.9	nd	This study



**FIG 6** Domain architectures and biochemical characterization of Xyn26A, Xyn10A, Xyn10B, and Xyn10C. Signal peptides were predicted by SignalP 5.0. Domain analysis was performed in the NCBI CDD database and the Pfam database. Enzyme activities were determined using the DNS method. nd, no detectable enzyme activity;  $T_{opt}$ , optimum temperature;  $pH_{opt}$ , optimum pH.

analyzed using high-performance anion-exchange chromatography equipped with a pulsed amperometric detector (HPAEC-PAD). The result showed that Xyn10A released xylose and  $\beta$ 1,4-xylobiose ( $\beta$ 1,4X2) from MLX, indicating that Xyn10A attacks both  $\beta$ 1,3- and  $\beta$ 1,4-linkages in MLX (Fig. 5A). Xyn10B released xylose,  $\beta$ 1,4X2,  $\beta$ 1,4X3, the mixed-linkage xylotriose X3X4X, and other unidentified mixed-linkage XOs (Fig. 5A). Xyn10C released xylose,  $\beta$ 1,4X2 and X3X4X (Fig. 5A). The presence of  $\beta$ 1,3-linkages in Xyn10B and Xyn10C products suggests that they attack  $\beta$ 1,4-linkages in MLX. Three GH10 xylanases from *Cryptococcus albidus*, *Streptomyces liuiduns*, and *Cryptococcus adeliae* have been reported to be able to hydrolyze MLX, which liberate from MLX a mixture containing X3X4X (30, 31), similar to Xyn10B and Xyn10C.

Consistent with the above *in vitro* biochemical analyses, xylose,  $\beta$ 1,4XOs (X2-X4),  $\beta$ 1,3X2, X3X4X, and other unidentified mixed-linkage XOs were detected in the culture supernatant of strain Q13 grown on MLX (Fig. 5B). This reflects a synergy of the extracellular xylanases Xyn10A, Xyn10B, Xyn10C, and Xyn26A on MLX degradation.

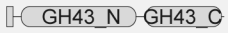



### Xylooligosaccharide degradation by periplasmic and cytoplasmic enzymes

The oligosaccharides generated by extracellular xylanases are transported across the outer membrane of bacterial cells by the SusC/D transporter system and further saccharified in the periplasm and the cytoplasm (13). Based on functional annotation and signal peptide prediction, XUL-Q13 encodes four putative XOs-degrading enzymes: the periplasmic Xyl43B and Xyl3A with type II signal peptides and the cytoplasmic Xyl43A and Rex10A that lack signal peptides (Fig. 2).

Both periplasmic Xyl43B and Xyl3A were annotated as  $\beta$ 1,4-xylosidases. Enzyme assays with recombinant Xyl43B and Xyl3A showed that in addition to  $\beta$ 1,4X2, they were capable of hydrolyzing  $\beta$ 1,3X2 (Fig. 7). With the culture supernatant of strain Q13 as the substrate, we simulated the enzymatic degradation process of XOs in the periplasm. Briefly, the culture supernatant of strain Q13 growing on MLX was incubated with xylosidases Xyl43B and Xyl3A separately, and the products were analyzed by HPAEC-PAD. The result showed that Xyl43B could degrade X3X4X and  $\beta$ 1,3X2, and Xyl3A could degrade all the XOs in the culture supernatant (Fig. 5C), indicating that Xyl3A and Xyl43B likely dedicate the complete hydrolysis of  $\beta$ 1,3-linkages in the periplasm of strain Q13. Two  $\beta$ 1,3-xylosidases have been reported so far, including XloA from *Vibrio* sp. XY-214 (40) and rSWU43A from *Streptomyces* sp. SWU10 (41); both are GH43 members. XloA is involved in  $\beta$ 1,3-xylan catabolism by *Vibrio* sp. XY-214, while the role of rSWU43A in *Streptomyces* sp. SWU10 is unknown (40, 41). So far, Xyl3A is the first GH3 xylosidase capable of degrading  $\beta$ 1,3-linkages.

The cytoplasmic Xyl43A was annotated as a  $\beta$ 1,4-xylosidase (Fig. 2). Substrate specificity analysis showed that Xyl43A exhibited strikingly high catalytic efficiency on  $\beta$ 1,4X2 but extremely low on  $\beta$ 1,3X2 ( $k_{cat}/K_m$  values of 51.0 s<sup>-1</sup> mM<sup>-1</sup> versus 0.001 s<sup>-1</sup>



Enzyme	Length (amino acid)	T <sub>opt</sub>	pH <sub>opt</sub>	Substrate	k <sub>cat</sub> /K <sub>m</sub> (s <sup>-1</sup> mM <sup>-1</sup> )
Xyl43B		40°C	5.0-6.0	β1,3X2	0.07
				β1,4X2	0.003
Xyl3A		30-40°C	7.0	β1,3X2	0.4
				β1,4X2	0.3
Xyl43A		40°C	7.0	β1,3X2	0.001
				β1,4X2	51.0
Rex10A		40°C	5.0-6.0	β1,3X2	nd
				β1,3X3	nd
				β1,4X2	nd
				β1,4X3	2.7
				β1,4X4	2.5
				β1,4X5	2.6
				β1,4X6	4.4

▮ Lipoprotein signal peptide (SPII)

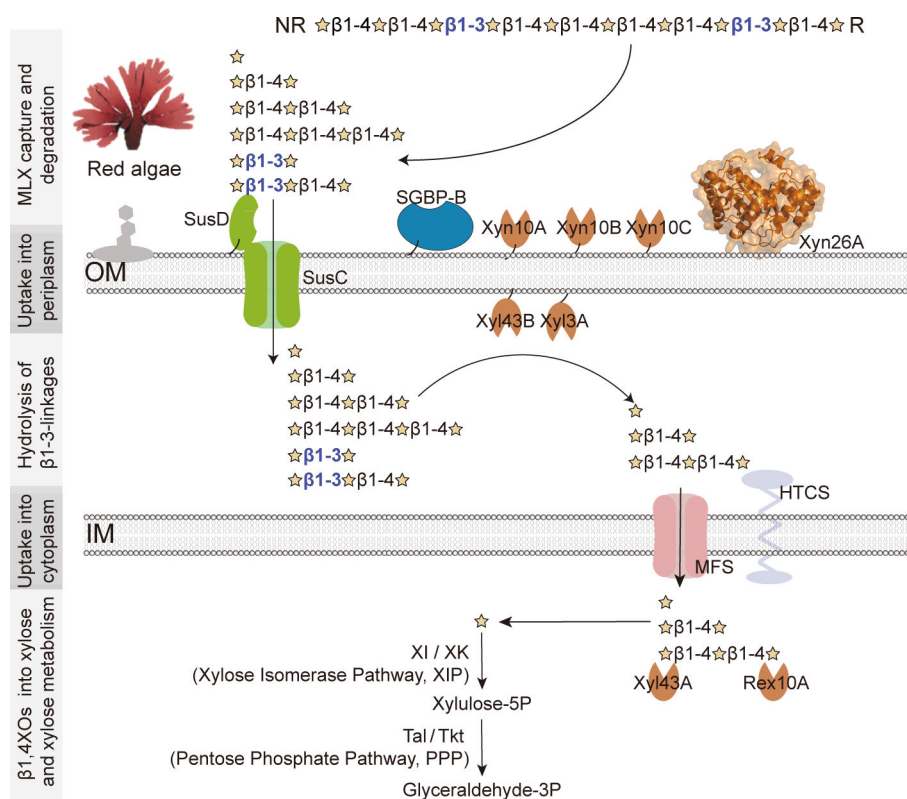
**FIG 7** Domain architectures and biochemical characterization of Xyl43B, Xyl3A, Xyl43A, and Rex10A. Enzyme activities were determined using the D-xylose kit.  $k_{cat}/K_m$  values were calculated by the Michaelis–Menten and Lineweaver–Burk fitting. When the Michaelis–Menten fitting and the Lineweaver–Burk fitting were not feasible, the  $k_{cat}/K_m$  value was calculated using the equation  $k_{cat}/K_m = V_0/[S]/[E]$ . The fitting curves are shown in Fig. S3.

mM<sup>-1</sup>) (Fig. 7; Fig. S3C), suggesting that Xyl43A is indeed a β1,4-xylosidase, a class of xylanolytic enzymes that release single xylose from the non-reducing end of β1,4XOs (42). Although Rex10A was annotated as a β1,4-xylanase, it showed no activity on any class of xylans (data not shown). Instead, Rex10A degraded β1,4XOs with the degrees of polymerization from three to six (β1,4X3–X6) with  $k_{cat}/K_m$  values of 2.5–4.4 s<sup>-1</sup> mM<sup>-1</sup>, but no activity on β1,3X2, β1,4X2, or β1,3X3 (Fig. 7; Fig. S3D), indicating that Rex10A is a β1,4-oligoxylanase. Moreover, Rex10A exhibited no activity on β1,4X3 reduced with NaBH<sub>4</sub> (Fig. 5D), indicating that Rex10A is a reducing-end xylose-releasing exo-oligoxylanase that attacks β1,4XOs from the reducing ends. This class of xylanolytic enzymes has been reported in one case in GH10 (43). Thus, in the cytoplasm of strain Q13, Xyl43A and Rex10A hydrolyze β1,4XOs from the non-reducing and reducing ends, respectively. In addition, their β1,4-specificity further supports that the β1,3-linkages are hydrolyzed before the XOs are transported into the cytoplasm.

Together, four XO-degrading enzymes are involved in the cascade saccharification of XOs by strain Q13, including Xyl43B, Xyl3A, Xyl43A, and Rex10A. Xyl43B and Xyl3A are scavengers of the β1,3-linkages in XOs in the periplasm, while Xyl43A and Rex10A take charge of the remaining β1,4-linkages in XOs in the cytoplasm.

### A model for MLX catabolism by *Polaribacter* sp. Q13

In summary of the above results, we proposed a working model in which a single XUL, XUL-Q13, enables strain Q13 to specifically utilize MLX (Fig. 8). This model involves MLX capture by SGBPs, MLX degradation by extracellular xylanases, transport of XOs through the outer membrane by SusC/D, hydrolysis of β1,3-linkages by periplasmic xylosidases, and the ultimate saccharification of β1,4XOs and assimilation of xylose by cytoplasmic enzymes (Fig. 8). Although it is analogous to the known XULs that target hetero-β1,4-xylans (11, 23–25), four characteristics underscore the MLX specificity: (i) SGBP-B mediates the capture specificity of strain Q13 to MLX. Cell-surface SGBPs are generally involved in the initial capture of polysaccharides (36, 37). In strain Q13,



**FIG 8** A model for MLX catabolism by strain Q13. Extracellularly, MLX is captured by SGBP-B and degraded by xylanases Xyn26A, Xyn10A, Xyn10B, and Xyn10C. The released xylooligosaccharides are transported into the periplasm via the SusC/D transporter complex, all  $\beta$ 1,3-linkages which are hydrolyzed by xylosidases Xyl43B and Xyl3A. The resultant  $\beta$ 1,4-xylooligosaccharides are transported into the cytoplasm via the MFS transporter and completely saccharified by  $\beta$ 1,4-xylosidase Xyl43A and reducing-end  $\alpha$ - $\beta$ 1,4-oligoxylanase Rex10A from the non-reducing and reducing ends, respectively. The produced xylose is metabolized through the xylose isomerase pathway and the pentose phosphate pathway.

although SGBP-A (PsSusD) is incompetent in xylan capture, SGBP-B prefers to bind MLX rather than hetero- $\beta$ 1,4-xylans, contributing to the MLX specificity. (ii) XUL-Q13 encodes an MLX-specific xylanase, Xyn26A. Xylan backbone is degraded by xylanases. To degrade hetero- $\beta$ 1,4-xylans, the reported XULs encode  $\beta$ 1,4-xylanases especially those from GH10 (11, 23–25). By comparison, the novel xylanase Xyn26A that specifically attacks MLX (27) is only present in XUL-Q13. Xyn26A can be taken as a hallmark to differentiate the MLX-specific XULs from the hetero- $\beta$ 1,4-xylan XULs. However, it is worth mentioning that this type of MLX-targeting XULs is not representative of all XULs that may be capable of MLX degradation (11). (iii) Xylosidases capable of degrading  $\beta$ 1,3-linkages are involved in the saccharification of XOs in the periplasm of strain Q13. The XOs that enter the periplasm of strain Q13 contain  $\beta$ 1,3-linkages. These  $\beta$ 1,3-linkages are hydrolyzed by xylosidases Xyl43B and Xyl3A, further underscoring the MLX specificity of XUL-Q13. (iv) Xylan-debranching enzyme is absent from XUL-Q13. To degrade hetero- $\beta$ 1,4-xylans, whose  $\beta$ 1,4-backbone is decorated with multiple side chains, a cardinal feature of bacterial hetero-XULs is the presence of a large diversity of xylanolytic enzymes. In addition to  $\beta$ 1,4-xylanases and  $\beta$ 1,4-xylosidases, debranching xylanolytic enzymes are required, such as  $\alpha$ 1,2-glucuronidases (GH67 and GH115),  $\alpha$ -L-galactosidase (GH95 and CE97), feruloyl esterases, and acetyl xylan esterases (CE1, CE6, and CE15) (Fig. 1B) (23–26, 44, 45). The lack of these enzymes in XUL-Q13 reflects the homogeneity (or the lack of modifications) of MLX targeted by this type of XULs.

Together, strain Q13 catabolizes MLX with a canonical Sus-like model, in which a cell surface glycan-binding protein and a unique xylanolytic enzyme system contribute to the catabolic specialization to MLX.

## Conclusion

*Polaribacter* sp. Q13 is a member of marine Bacteroidetes isolated from the surface of red algae, which specifically catabolizes MLX. Herein, we uncovered that the catabolic specialization of strain Q13 to MLX is based on an XUL, XUL-Q13. The cell surface glycan-binding protein SGBP-B mediates the capture specificity of strain Q13 toward MLX. The xylanolytic enzymatic cascade dedicates the complete hydrolysis of  $\beta$ 1,3- and  $\beta$ 1,4-linkages in MLX. Extracellularly, MLX is degraded by four xylanases including an MLX-specific xylanase that attacks precisely the  $\beta$ 1,4-linkages following a  $\beta$ 1,3-linkage. The  $\beta$ 1,3-linkages in the generated XOs are saccharified in the periplasm by two xylosidases. The residual  $\beta$ 1,4-linkages in the XOs are completely hydrolyzed in the cytoplasm by a  $\beta$ 1,4-xylosidase and a  $\beta$ 1,4-oligoxylanase. The generated xylose is finally assimilated through the xylose isomerase pathway and the pentose phosphate pathway. In addition, other marine Bacteroidetes strains harboring homologous MLX utilization loci also preferentially consume red algal MLX. This study sheds light on the catabolism of red algal MLX by marine Bacteroidetes.

## MATERIALS AND METHODS

### Materials

GX and AX,  $\beta$ 1,4XOs ( $\beta$ 1,4X2-X6) were purchased from Megazyme (Ireland). GAX and MLX were purchased from Elicityl (France).  $\beta$ 1,3-xylan,  $\beta$ 1,3X2,  $\beta$ 1,3X3, X3X4X, and X4X3X were prepared as previously described (27, 46). p-Nitrophenyl- $\beta$ -D-xylopyranoside (pNPX) was purchased from Sigma (USA).

### Growth assay

All bacterial strains, including *Polaribacter* sp. Q13 (GenBank: [CP074436.1](#)), *Polaribacter* sp. 11A2H (GenBank: [ASM1137902v1](#)), *Cellulophage* sp. 20\_2\_10 (GenBank: [ASM2347664v1](#)), *Cellulophage* sp. Z1A5H (GenBank: [ASM1137897v1](#)), *Algibacter* sp. L4\_22 (GenBank: [ASM2347304v1](#)), and *Aureibaculum luteum* SM1352 (GenBank: [ASM344901v1](#)), were all grown at 20°C in the minimal medium (27) supplemented with 0.2% (wt/vol) carbon source under aerobic conditions. The carbon sources included MLX, GX, AX, GAX, xylose, and glucose. Growth was monitored by measuring OD<sub>600</sub>, and an increase of OD<sub>600</sub> ( $\Delta$ OD<sub>600</sub>) was generated to compare the bacterial growth on different carbon sources (27, 47).

### Transcriptome analysis

Strain Q13 was cultivated in duplicate in a 20 mL minimal medium containing 0.2% (wt/vol) MLX, xylose, or glucose for 36–48 h to their mid-log phase. Then, cells were harvested separately (4,000 g for 10 min at 4°C), and the total RNA was extracted using the TRIzol reagent (Invitrogen, USA). After the genomic DNA was removed using DNase I (Takara, Japan), 4  $\mu$ g RNA from each sample was used to prepare RNA-seq strand-specific libraries with the TruSeq RNA sample preparation kit (Illumina, USA) and RiboZero rRNA removal kit (Epicenter, USA). High-throughput sequencing was performed in paired-end reads on an Illumina HiSeq 6000 platform in Shanghai BIOZERO (China), and the clean reads were separately aligned to the strain Q13 reference genome using Rockhopper (<http://cs.wellesley.edu/~btjaden/Rockhopper/>). The differential gene expression analysis was performed with edgeR (<https://bioconductor.org/packages/release/bioc/html/edgeR.html>), and the transcript levels were compared based on the RPKM method (48).

## Proteome analysis

Strain Q13 was cultivated in triplicate in a 20-mL minimal medium containing 0.2% (wt/vol) MLX, xylose, or glucose for 36–48 h to the mid-log phase (27). Then, cells were collected separately (4,000 *g* for 10 min at 4°C) for proteome analysis in Shanghai Applied Protein Technology (China). In brief, the SDT buffer (4% SDS, 1 mM DTT, 100 mM Tris-HCl, pH 7.6) was used for sample lysis and protein extraction. After quantification with a Pierce bicinchoninic acid protein assay kit (Thermo, USA), 200- $\mu$ g proteins from each sample were digested with trypsin according to the filter-aided sample preparation procedure (49). The released peptides were separated with a reversed-phase C18 column. Mass spectrometry (MS) and MS/MS data were determined using a Q Exactive mass spectrometer (Thermo, USA). MS spectra were analyzed with MaxQuant (50). Proteins that were detected in at least two out of three biological replicates were counted as identified. Based on the iBAQ values from MaxQuant analysis, the riBAQ values of each protein were calculated for semi-quantitative comparisons (6). The riBAQ values were then averaged and log-transformed and termed log<sub>2</sub> ratios.

## Gene cloning and protein production

Gene cloning and protein production were carried out as previously described (27). In brief, genes encoding SGBP-B, Xyl43A, Xyn10A, Xyn10B, Xyn26A, Xyl43B, Rex10A, Xyn10C, and Xyl3A were cloned from the genomic DNA of strain Q13 by PCR amplification and inserted into the pET22b vector (Novagen, USA). The primers used are shown in Table S1. The constructed plasmids were transferred into *E. coli* BL21 (DE3) for protein production. Xyl43B and Rex10A were partially produced as soluble forms with inclusion bodies also being observed, and all the other proteins were exclusively produced as soluble forms. Recombinant proteins were purified by Ni<sup>2+</sup>-nitrilotriacetic acid resin (GE Healthcare, USA) and then fractionated by SEC on a Superdex G200 column (GE Healthcare, USA). The protein purity was determined with SDS-PAGE. Protein concentrations were determined by a bicinchoninic acid protein assay kit (Thermo Fisher Scientific) with bovine serum albumin as the standard.

## Isothermal titration calorimetry

ITC measurements were performed with MicroCal PEAQ-ITC (Malvern, United Kingdom) at 25°C in 50 mM Tris-HCl (pH 8.0) containing 100 mM NaCl. The concentration of SGBP-B and ligands (MLX, GX, and AX) was 50  $\mu$ M and 5 mg/mL, respectively. Each ligand was injected into the protein cell 19 times with a stirring speed of 800 rpm. The first injection was 0.4  $\mu$ L, and the following 18 injections were 3.0  $\mu$ L. The data were analyzed with Microcal PEAQ-ITC analysis software. The molar concentration of xylans was estimated to fit  $N$  (binding site) = 1 (51).

## Enzyme assays

Unless otherwise noted, the activities of enzymes were performed in phosphate-buffered saline (PBS, 20 mM) under their respective optimum pHs and optimum temperatures. With xylans as the substrates, enzyme activities were determined using the DNS method (27). With XOs as the substrates, enzyme activities were determined by quantifying the produced xylose using the D-xylose kit (Megazyme, Ireland). Reactions were initiated by adding a 10- $\mu$ L enzyme solution to a 90  $\mu$ L mixture of NAD<sup>+</sup>, ATP, hexokinase, xylose mutarotase, xylose dehydrogenase, and XO substrates. After 10-min incubation, reactions were terminated by 150  $\mu$ L Na<sub>2</sub>CO<sub>3</sub> (1 M). Then, the NADH absorbance at 340 nm was measured. The standard curve was generated with xylose (0–60  $\mu$ M). With pNPX as the substrate, the 200- $\mu$ L reaction mixture contained a 10- $\mu$ L enzyme solution and 190- $\mu$ L pNPX (2 mM). After a 10-min incubation, 200  $\mu$ L Na<sub>2</sub>CO<sub>3</sub> (1 M) was added, and the p-nitrophenyl (pNP) absorbance at 405 nm was measured. The

standard curve was generated with pNP (0–200  $\mu\text{M}$ ). One unit (U) was defined as the amount of enzyme required to release 1  $\mu\text{mol}$  xylose or pNP per minute.

### Enzymatic characterization and kinetics

Enzyme characterization was performed with MLX,  $\beta\text{1,4X3}$ , and pNPX as the substrate for xylanases (Xyn10A, Xyn10B, and Xyn10C), exo-oligoxyranase (Rex10A), and xylosidases (Xyl3A, Xyl43A, and Xyl43B), respectively. The effect of temperature was determined ranging from 0°C to 60°C at an interval of 10°C. The effect of pH was determined with the Britton–Robinson buffer (40 mM) from pH 4.0 to 10.0. Substrate specificities of xylanases Xyn10A, Xyn10B, and Xyn10C were determined with MLX, GX, AX, and  $\beta\text{1,3-xylan}$  (10 mg/mL each) as the substrates. The kinetics of Xyl43A, Xyl43B, Xyl3A, and Rex10A were determined by Michaelis–Menten and Lineweaver–Burk fitting based on initial rates assayed with different concentrations of substrates. When saturation was not attained, the catalytic efficiency ( $k_{\text{cat}}/K_{\text{m}}$ ) was directly given using the equation  $k_{\text{cat}}/K_{\text{m}} = V_0/[S]/[E]$  (23, 45).

### Modes of action analysis of xylanases

Time-course assays of xylanases Xyn10A, Xyn10B, and Xyn10C were performed as previously described (27). Reaction mixtures containing 90  $\mu\text{L}$  MLX (5 mg/mL) and 10  $\mu\text{L}$  each of xylanases Xyn10A (0.5 mg/mL), Xyn10B (2.4 mg/mL), and Xyn10C (0.6 mg/mL) were incubated in PBS (under their respective optimum pH) at 30°C. The products of each xylanase after 24 h hydrolysis were diluted ( $10^{-2}$ – $10^{-3}$  dilution) with ultrapure water and analyzed by HPAEC-PAD.

### Mode of action analysis of Rex10A

For the time-course assay, the reaction mixture containing 140  $\mu\text{L}$   $\beta\text{1,4X6}$  (50  $\mu\text{M}$ ) and 10  $\mu\text{L}$  Rex10A (0.2 mg/mL) in PBS (pH 6.0) was incubated at 30°C. At different time points within 1 h, the reaction was terminated by 150  $\mu\text{L}$  NaOH (30 mM), and the products were analyzed by HPAEC-PAD. To determine the activity of Rex10A on the reduced  $\beta\text{1,4X3}$ ,  $\beta\text{1,4X3}$  was reduced by  $\text{NaBH}_4$  according to the method of Leth et al. (45) with minor modifications. In brief, 10  $\mu\text{L}$   $\text{NaBH}_4$  (1 M in 200 mM NaOH) was added into 40  $\mu\text{L}$   $\beta\text{1,4X3}$  (40 mM). After incubation on ice for 1 h, the reaction was quenched by 10  $\mu\text{L}$  acetic acid (1 M), and the mixture was diluted 10-fold in PBS (pH 6.0). As a control, 200 mM NaOH was used instead of  $\text{NaBH}_4$ . Then, 90  $\mu\text{L}$  reduced  $\beta\text{1,4X3}$  was mixed with 10  $\mu\text{L}$  Rex10A (1.0 mg/mL) in PBS (pH 6.0), and the mixture was incubated at 40°C for 10 min. The reaction was terminated by boiling for 5 min, and the products were analyzed using TLC, which was performed on the silica gel 60 F254 plate (Sigma, USA). The solvent system was 1-butanol–acetic acid–ultrapure water [13:12:2 (vol/vol/vol)]. XOs were visualized by sulfuric acid–ethanol [1:10 (vol/vol)] after incubation at 100°C for 10 min.

### *In vivo* assay for MLX degradation

Strain Q13 was cultivated in the minimal medium containing 0.2% (wt/vol) MLX for 36–48 h to the mid-log phase. After centrifugation (4,000  $g$  for 10 min at 4°C), the culture supernatant was collected, filtered with a 0.22  $\mu\text{m}$  filter, and diluted 20-fold with ultrapure water. Then, XOs in the supernatant were analyzed with HPAEC-PAD. The culture supernatant was then hydrolyzed by xylosidases Xyl43B and Xyl3A separately. The reaction mixture containing 140  $\mu\text{L}$  diluted supernatant and 10  $\mu\text{L}$  enzyme solution (1 mg/mL each) was incubated at 40°C for 10 min and terminated by 150  $\mu\text{L}$  NaOH (30 mM). After filtration with 0.22  $\mu\text{m}$  filters, the samples were injected into HPAEC-PAD for XO analysis.

## High-performance anion-exchange chromatography equipped with a pulsed amperometric detector

HPAEC-PAD was carried out using an ICS-6000 machine equipped with a CarboPac PA200 column (Thermo, USA). Solvents and elution programs were described previously (27). Xylose,  $\beta$ 1,4XOs ( $\beta$ 1,4X2-X6),  $\beta$ 1,3XOs ( $\beta$ 1,3X2-X3), X3X4X, and X4X3X were used as standards to identify the peaks in chromatograms.

### Bioinformatics

Signal peptides were predicted using SignalP 5.0 (52) and LipoP 1.0 (53). Domain analysis was performed in the NCBI Conserved Domain Database (54) and the Pfam database (55). For XUL comparison, sequence alignments were performed with BLAST+ (version 2.7.1+,  $E$ -value  $1e-5$ ). The genes and their synteny were drawn with genoPlotR 0.8.9 (56). Xyn26A homologs were searched in the IMG/M database (<https://img.jgi.doe.gov/m/>) (35) against all available bacterial genomes using BLASTP with a stringency of 35% identity and a cut-off value of  $1e-50$  (35). Heatmaps were drawn with TBtools (<https://github.com/CJ-Chen/TBtools/releases>) (57).

### ACKNOWLEDGMENTS

We thank Cai-Yun Sun and Xiang-Mei Ren from the State Key Laboratory of Microbial Technology of Shandong University for their help and guidance with HPLC and HPAEC-PAD.

This work was supported by the National Key Research and Development Program (2022YFC2807500 and 2022YFC2807503), the Marine S&T Fund of Shandong Province for Qingdao Marine Science and Technology Center (2022QNL030004-3), the National Science Foundation of China (U2006205, 31961133016, 42306166, and 32200018), the Program of Shandong for Taishan Scholars (tspd20181203), and the Natural Science Foundation of Shandong Province, China (ZR2021QC024).

N.W., Y.Y., and X.-L.C. conceived and guided the study. F.Z., C.-M.Y., H.-N.S., and T.-T.X. performed the experiments. Z.-Z.S. advised on the bioinformatics analysis. F.Z. and N.W. wrote the manuscript. X.-L.C., Y.Y., Q.-L.Q., and Y.-Z.Z. revised the manuscript. All authors approved the final version of the manuscript.

### AUTHOR AFFILIATIONS

<sup>1</sup>Marine Biotechnology Research Center, State Key Laboratory of Microbial Technology, Shandong University, Qingdao, China

<sup>2</sup>College of Marine Life Sciences & Frontiers Science Center for Deep Ocean Multispheres and Earth System, Ocean University of China, Qingdao, China

<sup>3</sup>Laboratory for Marine Biology and Biotechnology, Laoshan Laboratory, Qingdao, China

### AUTHOR ORCIDs

Fang Zhao  <http://orcid.org/0000-0003-2991-3631>

Ning Wang  <http://orcid.org/0000-0001-5420-8040>

Xiu-Lan Chen  <http://orcid.org/0000-0001-7755-5977>

Yang Yu  <http://orcid.org/0000-0002-0774-4059>

Yu-Zhong Zhang  <http://orcid.org/0000-0002-2017-1005>

### FUNDING

Funder	Grant(s)	Author(s)
<a href="#">MOST   National Key Research and Development Program of China (NKPs)</a>	2022YFC2807500, 2022YFC2807503	Qi-Long Qin

Funder	Grant(s)	Author(s)
Marine S&T Fund of Shandong Province for Qingdao Marine Science and Technology Center	2022QNLM030004-3	Yu-Zhong Zhang
National Science Foundation (NSF)	U2006205, 31961133016, 32200018	Xiu-Lan Chen
Program of Shandong foTaishan Scholars	tspd20181203	Yu-Zhong Zhang
山东省科学技术厅   Natural Science Foundation of Shandong Province (山东省自然科学基金)	ZR2021QC024	Fang Zhao

## DATA AVAILABILITY

The RNA-seq data are available in the NCBI SRA database under the accession number [PRJNA844361](https://www.ncbi.nlm.nih.gov/sra/PRJNA844361). The mass spectrometry proteome data were deposited to the ProteomeXchange Consortium via the PRIDE partner repository with the dataset identifier [PXD035342](https://www.ebi.ac.uk/pride/archive/dataset/PXD035342).

## ADDITIONAL FILES

The following material is available [online](#).

### Supplemental Material

**Fig. S1 to S3, Table S1 (AEM01704-23-s0001.docx).** Fig. S1 (SDS-PAGE) S2 (HPLC chromatograms), and S3 (Enzymatic kinetics fitting curves) and Table S1 (Primer sequences).

## REFERENCES

1. Hehemann JH, Boraston AB, Czjzek M. 2014. A sweet new wave: structures and mechanisms of enzymes that digest polysaccharides from marine algae. *Curr Opin Struct Biol* 28:77–86. <https://doi.org/10.1016/j.sbi.2014.07.009>
2. Field CB, Behrenfeld MJ, Randerson JT, Falkowski P. 1998. Primary production of the biosphere: integrating terrestrial and oceanic components. *Science* 281:237–240. <https://doi.org/10.1126/science.281.5374.237>
3. Arnosti C, Wietz M, Brinkhoff T, Hehemann JH, Probandt D, Zeugner L, Amann R. 2021. The biogeochemistry of marine polysaccharides: sources, inventories, and bacterial drivers of the carbohydrate cycle. *Ann Rev Mar Sci* 13:81–108. <https://doi.org/10.1146/annurev-marine-032020-012810>
4. Kumar M, Sun YQ, Rathour R, Pandey A, Thakur IS, Tsang DCW. 2020. Algae as potential feedstock for the production of biofuels and value-added products: opportunities and challenges. *Sci Total Environ* 716:137116. <https://doi.org/10.1016/j.scitotenv.2020.137116>
5. Müller C, Scapini T, Rempel A, Abaide ER, Camargo AF, Nazari MT, Tadioto V, Bonatto C, Tres MV, Zobot GL, Colla LM, Treichel H, Alves SL. 2023. Challenges and opportunities for third-generation ethanol production: a critical review. *Eng Microbiol* 3:100056. <https://doi.org/10.1016/j.engmic.2022.100056>
6. Unfried F, Becker S, Robb CS, Hehemann J-H, Markert S, Heiden SE, Hinzke T, Becher D, Reintjes G, Krüger K, Avci B, Kappelmann L, Hahnke RL, Fischer T, Harder J, Teeling H, Fuchs B, Barbeyron T, Amann RI, Schweder T. 2018. Adaptive mechanisms that provide competitive advantages to marine Bacteroidetes during microalgal blooms. *ISME J* 12:2894–2906. <https://doi.org/10.1038/s41396-018-0243-5>
7. Reisky L, Préchoux A, Zühlke M-K, Bäumgen M, Robb CS, Gerlach N, Roret T, Stanetty C, Larocque R, Michel G, Song T, Markert S, Unfried F, Mihovilovic MD, Trautwein-Schult A, Becher D, Schweder T, Bornscheuer UT, Hehemann J-H. 2019. A marine bacterial enzymatic cascade degrades the algal polysaccharide ulvan. *Nat Chem Biol* 15:803–812. <https://doi.org/10.1038/s41589-019-0311-9>
8. Chen J, Robb CS, Unfried F, Kappelmann L, Markert S, Song T, Harder J, Avci B, Becher D, Xie P, Amann RI, Hehemann J-H, Schweder T, Teeling H. 2018. Alpha- and beta-mannan utilization by marine Bacteroidetes. *Environ Microbiol* 20:4127–4140. <https://doi.org/10.1111/1462-2920.14414>
9. Thomas F, Barbeyron T, Tonon T, Génicot S, Czjzek M, Michel G. 2012. Characterization of the first alginolytic operons in a marine bacterium: from their emergence in marine *Flavobacteriia* to their independent transfers to marine Proteobacteria and human gut Bacteroides. *Environ Microbiol* 14:2379–2394. <https://doi.org/10.1111/j.1462-2920.2012.02751.x>
10. Ficko-Blean E, Préchoux A, Thomas F, Rochat T, Larocque R, Zhu Y, Stam M, Génicot S, Jam M, Calteau A, Viart B, Ropartz D, Pérez-Pascual D, Correc G, Matard-Mann M, Stubbs KA, Rogniaux H, Jeudy A, Barbeyron T, Médigue C, Czjzek M, Vallenet D, McBride MJ, Duchaud E, Michel G. 2017. Carrageenan catabolism is encoded by a complex regulon in marine heterotrophic bacteria. *Nat Commun* 8:1685. <https://doi.org/10.1038/s41467-017-01832-6>
11. Dutschei T, Beidler I, Bartosik D, Seeßelberg J-M, Teune M, Bäumgen M, Ferreira SQ, Heldmann J, Nagel F, Krull J, Berndt L, Methling K, Hein M, Becher D, Langer P, Delcea M, Lalk M, Lammers M, Höhne M, Hehemann J-H, Schweder T, Bornscheuer UT. 2023. Marine Bacteroidetes enzymatically digest xylans from terrestrial plants. *Environ Microbiol* 25:1713–1727. <https://doi.org/10.1111/1462-2920.16390>
12. Fernández-Gómez B, Richter M, Schüler M, Pinhassi J, Acinas SG, González JM, Pedrós-Alió C. 2013. Ecology of marine Bacteroidetes: a comparative genomics approach. *ISME J* 7:1026–1037. <https://doi.org/10.1038/ismej.2012.169>
13. Martens EC, Koropatkin NM, Smith TJ, Gordon JI. 2009. Complex glycan catabolism by the human gut microbiota: the Bacteroidetes sus-like paradigm. *J Biol Chem* 284:24673–24677. <https://doi.org/10.1074/jbc.R109.022848>

14. Usov AI, Zelinsky ND. 2013. Chemical structures of algal polysaccharides, p 23–86. In Dominguez H (ed), *Functional ingredients from algae for foods and nutraceuticals*. Elsevier, Cambridge, UK.
15. Hansell DA, Kadko D, Bates NR. 2004. Degradation of terrigenous dissolved organic carbon in the Western Arctic ocean. *Science* 304:858–861. <https://doi.org/10.1126/science.1096175>
16. Scheller HV, Ulvskov P. 2010. Hemicelluloses. *Annu Rev Plant Biol* 61:263–289. <https://doi.org/10.1146/annurev-arplant-042809-112315>
17. Burton RA, Gidley MJ, Fincher GB. 2010. Heterogeneity in the chemistry, structure and function of plant cell walls. *Nat Chem Biol* 6:724–732. <https://doi.org/10.1038/nchembio.439>
18. Iriki Y, Suzuki T, Nisizawa K, Miwa T. 1960. Xylan of siphonaceous green algae. *Nature* 187:82–83. <https://doi.org/10.1038/187082a0>
19. Turvey JR, Williams EL. 1970. Structures of some xylans from red algae. *Phytochemistry* 9:2383–2388. [https://doi.org/10.1016/S0031-9422\(00\)85744-1](https://doi.org/10.1016/S0031-9422(00)85744-1)
20. Lahaye M, Rondeau-Mouro C, Deniaud E, Buléon A. 2003. Solid-state <sup>13</sup>C NMR spectroscopy studies of xylans in the cell wall of *Palmaria palmata* (L. Kuntze, Rhodophyta). *Carbohydr Res* 338:1559–1569. [https://doi.org/10.1016/S0008-6215\(03\)00241-6](https://doi.org/10.1016/S0008-6215(03)00241-6)
21. Viana AG, Nosedá MD, Gonçalves AG, Duarte MER, Yokoya N, Matulewicz MC, Cerezo AS. 2011. β-D-(1→4), β-D-(1→3) 'mixed linkage' xylans from red seaweeds of the order *Nemaliales* and *Palmariales*. *Carbohydr Res* 346:1023–1028. <https://doi.org/10.1016/j.carres.2011.03.013>
22. Hsieh YSY, Harris PJ. 2019. Xylans of red and green algae: what is known about their structures and how they are synthesised? *Polymers (Basel)* 11:354. <https://doi.org/10.3390/polym11020354>
23. Rogowski A, Briggs JA, Mortimer JC, Tryfona T, Terrapon N, Lowe EC, Baslé A, Morland C, Day AM, Zheng H, Rogers TE, Thompson P, Hawkins AR, Yadav MP, Henrissat B, Martens EC, Dupree P, Gilbert HJ, Bolam DN. 2015. Glycan complexity dictates microbial resource allocation in the large intestine. *Nat Commun* 6:7481. <https://doi.org/10.1038/ncomms8481>
24. Dodd D, Moon YH, Swaminathan K, Mackie RI, Cann IKO. 2010. Transcriptomic analyses of xylan degradation by *Prevotella bryantii* and insights into energy acquisition by xylanolytic Bacteroidetes. *J Biol Chem* 285:30261–30273. <https://doi.org/10.1074/jbc.M110.141788>
25. Tang K, Lin Y, Han Y, Jiao N. 2017. Characterization of potential polysaccharide utilization systems in the marine Bacteroidetes *Gramella flava* JLT2011 using a multi-omics approach. *Front Microbiol* 8:220. <https://doi.org/10.3389/fmicb.2017.00220>
26. Despres J, Forano E, Lepercq P, Comtet-Marre S, Jubelin G, Chambon C, Yeoman CJ, Berg Miller ME, Fields CJ, Martens E, Terrapon N, Henrissat B, White BA, Mosoni P. 2016. Xylan degradation by the human gut *Bacteroides xylanisolvens* XB1A(T) involves two distinct gene clusters that are linked at the transcriptional level. *BMC Genomics* 17:326. <https://doi.org/10.1186/s12864-016-2680-8>
27. Zhao F, Yu CM, Sun HN, Zhao LS, Ding HT, Cao HY, Chen Y, Qin QL, Zhang YZ, Li PY, Chen XL. 2023. A novel class of xylanases specifically degrade marine red algal β1,3/1,4-mixedlinkage xylan. *J Biol Chem* 299:105116. <https://doi.org/10.1016/j.jbc.2023.105116>
28. Tamura K, Hemsworth GR, Déjean G, Rogers TE, Pudlo NA, Urs K, Jain N, Davies GJ, Martens EC, Brumer H. 2017. Molecular mechanism by which prominent human gut Bacteroidetes utilize mixed-linkage β-glucans, major health-promoting cereal polysaccharides. *Cell Rep* 21:2030. <https://doi.org/10.1016/j.celrep.2017.11.013>
29. Chen WP, Matsuo M, Yasui T. 1986. β-1,3-xylanase and β-1,4-xylanase action on rhodymenan. *Agric Biol Chem* 50:1195–1200. <https://doi.org/10.1080/00021369.1986.10867544>
30. Biely P, Vrsanská M, Tenkanen M, Kluepfel D. 1997. Endo-β-1,4-xylanase families: differences in catalytic properties. *J Biotechnol* 57:151–166. [https://doi.org/10.1016/S0168-1656\(97\)00096-5](https://doi.org/10.1016/S0168-1656(97)00096-5)
31. Nerinckx W, Broberg A, Duus JØ, Ntarima P, Parolis LAS, Parolis H, Claeysens M. 2004. Hydrolysis of *Nothogenia erinacea* xylan by xylanases from families 10 and 11. *Carbohydr Res* 339:1047–1060. <https://doi.org/10.1016/j.carres.2004.02.017>
32. Lombard V, Golaconda Ramulu H, Drula E, Coutinho PM, Henrissat B. 2014. The carbohydrate-active enzymes database (CAZy) in 2013. *Nucleic Acids Res* 42:D490–D495. <https://doi.org/10.1093/nar/gkt1178>
33. Li X, Chen Y, Nielsen J. 2019. Harnessing xylose pathways for biofuels production. *Curr Opin Biotechnol* 57:56–65. <https://doi.org/10.1016/j.copbio.2019.01.006>
34. Jagtap SS, Rao CV. 2018. Microbial conversion of xylose into useful bioproducts. *Appl Microbiol Biotechnol* 102:9015–9036. <https://doi.org/10.1007/s00253-018-9294-9>
35. Chen I-MA, Chu K, Palaniappan K, Ratner A, Huang J, Huntemann M, Hajek P, Ritter S, Varghese N, Seshadri R, Roux S, Woyke T, Eloe-Fadrosh EA, Ivanova NN, Kyrpides NC. 2021. The IMG/M data management and analysis system v.6.0: new tools and advanced capabilities. *Nucleic Acids Res* 49:D751–D763. <https://doi.org/10.1093/nar/gkaa939>
36. Kappelmann L, Krüger K, Hehemann J-H, Harder J, Markert S, Unfried F, Becher D, Shapiro N, Schweder T, Amann RI, Teeling H. 2019. Polysaccharide utilization loci of North Sea Flavobacteria as basis for using SusC/D-protein expression for predicting major phytoplankton glycans. *ISME J* 13:76–91. <https://doi.org/10.1038/s41396-018-0242-6>
37. Déjean G, Tamura K, Cabrera A, Jain N, Pudlo NA, Pereira G, Viborg AH, Van Petegem F, Martens EC, Brumer H. 2020. Synergy between cell surface glycosidases and glycan-binding proteins dictates the utilization of specific β(1,3)-glucans by human gut Bacteroides. *mBio* 11:e00095-20. <https://doi.org/10.1128/mBio.00095-20>
38. Bågenholm V, Reddy SK, Bouraoui H, Morrill J, Kulcinskaja E, Bahr CM, Aurelius O, Rogers T, Xiao Y, Logan DT, Martens EC, Koropatkin NM, Stålbrand H. 2017. Galactomannan catabolism conferred by a polysaccharide utilization locus of *Bacteroides ovatus*: enzyme synergy and crystal structure of a β-mannanase. *J Biol Chem* 292:229–243. <https://doi.org/10.1074/jbc.M116.746438>
39. Tausin AS, Wang Z, Cioci G, Li X, Labourel A, Machado B, Lippens G, Potocki-Veronese G, Young VB. 2022. Structural and biochemical characterization of a nonbinding SusD-like protein involved in xylooligosaccharide utilization by an uncultured human gut *Bacteroides* strain. *mSphere* 7:e0024422. <https://doi.org/10.1128/msphere.00244-22>
40. Umemoto Y, Onishi R, Araki T. 2008. Cloning of a novel gene encoding β-1,3-xylosidase from a marine bacterium, *Vibrio* sp. strain XY-214, and characterization of the gene product. *Appl Environ Microbiol* 74:305–308. <https://doi.org/10.1128/AEM.01793-07>
41. Phuenngmaung P, Fujiwara D, Sukhumsirichart W, Sakamoto T. 2018. Identification and characterization of the first β-1,3-D-xylosidase from a gram-positive bacterium, *Streptomyces* sp. *Enzyme Microb Technol* 112:72–78. <https://doi.org/10.1016/j.enzmictec.2017.11.002>
42. Rohman A, Dijkstra BW, Pusaningsih NNT. 2019. β-xylosidases: structural diversity, catalytic mechanism, and inhibition by monosaccharides. *Int J Mol Sci* 20:5524. <https://doi.org/10.3390/ijms20225524>
43. Santos CR, Hoffmam ZB, de Matos Martins VP, Zanphorlin LM, de Paula Assis LH, Honorato RV, Lopes de Oliveira PS, Ruller R, Murakami MT. 2014. Molecular mechanisms associated with xylan degradation by *Xanthomonas* plant pathogens. *J Biol Chem* 289:32186–32200. <https://doi.org/10.1074/jbc.M114.605105>
44. Déjean G, Blanvillain-Baufumé S, Boulanger A, Darrasse A, de Bernonville TD, Girard A-L, Carrère S, Jamet S, Zischek C, Lautier M, Solé M, Büttner D, Jacques M-A, Lauber E, Arlat M. 2013. The xylan utilization system of the plant pathogen *Xanthomonas campestris* pv *campestris* controls epiphytic life and reveals common features with oligotrophic bacteria and animal gut symbionts. *New Phytol* 198:899–915. <https://doi.org/10.1111/nph.12187>
45. Leth ML, Ejby M, Workman C, Ewald DA, Pedersen SS, Sternberg C, Bahl MI, Licht TR, Aachmann FL, Westereng B, Abou Hachem M. 2018. Differential bacterial capture and transport preferences facilitate co-growth on dietary xylan in the human gut. *Nat Microbiol* 3:570–580. <https://doi.org/10.1038/s41564-018-0132-8>
46. Sun HN, Yu CM, Fu HH, Wang P, Fang ZG, Zhang YZ, Chen XL, Zhao F. 2021. Diversity of marine 1,3-xylan-utilizing bacteria and characters of their extracellular 1,3-xylanases. *Front Microbiol* 12:721422. <https://doi.org/10.3389/fmicb.2021.721422>
47. Martens EC, Lowe EC, Chiang H, Pudlo NA, Wu M, McNulty NP, Abbott DW, Henrissat B, Gilbert HJ, Bolam DN, Gordon JI, Eisen JA. 2011. Recognition and degradation of plant cell wall polysaccharides by two human gut symbionts. *PLoS Biol* 9:e1001221. <https://doi.org/10.1371/journal.pbio.1001221>



48. Mortazavi A, Williams BA, McCue K, Schaeffer L, Wold B. 2008. Mapping and quantifying mammalian transcriptomes by RNA-Seq. *Nat Methods* 5:621–628. <https://doi.org/10.1038/nmeth.1226>
49. Wiśniewski JR, Zougman A, Nagaraj N, Mann M. 2009. Universal sample preparation method for proteome analysis. *Nat Methods* 6:359–362. <https://doi.org/10.1038/nmeth.1322>
50. Tyanova S, Temu T, Cox J. 2016. The MaxQuant computational platform for mass spectrometry-based shotgun proteomics. *Nat Protoc* 11:2301–2319. <https://doi.org/10.1038/nprot.2016.136>
51. Zolotnitsky G, Cogan U, Adir N, Solomon V, Shoham G, Shoham Y. 2004. Mapping glycoside hydrolase substrate subsites by isothermal titration calorimetry. *Proc Natl Acad Sci U S A* 101:11275–11280. <https://doi.org/10.1073/pnas.0404311101>
52. Almagro Armenteros JJ, Tsirigos KD, Sønderby CK, Petersen TN, Winther O, Brunak S, von Heijne G, Nielsen H. 2019. SignalP 5.0 improves signal peptide predictions using deep neural networks. *Nat Biotechnol* 37:420–423. <https://doi.org/10.1038/s41587-019-0036-z>
53. Juncker AS, Willenbrock H, Von Heijne G, Brunak S, Nielsen H, Krogh A. 2003. Prediction of lipoprotein signal peptides in Gram-negative bacteria. *Protein Sci* 12:1652–1662. <https://doi.org/10.1110/ps.0303703>
54. Marchler-Bauer A, Bo Y, Han L, He J, Lanczycki CJ, Lu S, Chitsaz F, Derbyshire MK, Geer RC, Gonzales NR, Gwadz M, Hurwitz DI, Lu F, Marchler GH, Song JS, Thanki N, Wang Z, Yamashita RA, Zhang D, Zheng C, Geer LY, Bryant SH. 2017. CDD/SPARCLE: functional classification of proteins via subfamily domain architectures. *Nucleic Acids Res* 45:D200–D203. <https://doi.org/10.1093/nar/gkw1129>
55. Mistry J, Chuguransky S, Williams L, Qureshi M, Salazar GA, Sonnhammer ELL, Tosatto SCE, Paladin L, Raj S, Richardson LJ, Finn RD, Bateman A. 2021. Pfam: the protein families database in 2021. *Nucleic Acids Res* 49:D412–D419. <https://doi.org/10.1093/nar/gkaa913>
56. Guy L, Roat Kultima J, Andersson SGE. 2010. genoPlotR: comparative gene and genome visualization in R. *Bioinformatics* 26:2334–2335. <https://doi.org/10.1093/bioinformatics/btq413>
57. Chen C, Chen H, Zhang Y, Thomas HR, Frank MH, He Y, Xia R. 2020. TBtools: an integrative toolkit developed for interactive analyses of big biological data. *Mol Plant* 13:1194–1202. <https://doi.org/10.1016/j.molp.2020.06.009>